

Study of Ion Velocity Effect on the Band Gap of CVD-Grown Few-Layer MoS₂

Mayur Khan,* Ramcharan Meena, Devesh Kumar Avasthi, and Ambuj Tripathi

Cite This: *ACS Omega* 2023, 8, 46540–46547

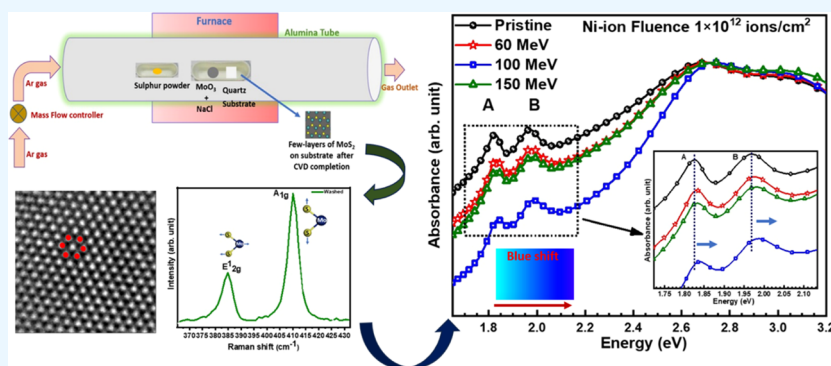
Read Online

ACCESS |

Metrics & More

Article Recommendations

Supporting Information



ABSTRACT: The present work reports on a simple chemical vapor deposition (CVD) technique that employs alkali halide (NaCl) to synthesize high-quality few-layer MoS₂ by reducing growth temperature from 850 to 650 °C, and its ion irradiation study for band gap modification. The Raman peak position difference of A_{1g} to E_{2g} of ≈ 24.5 cm⁻¹ for the synthesized MoS₂ corresponds to a few layers (<5 monolayers) of MoS₂ on the substrate, as also confirmed by atomic force microscopy (AFM). The optical image shows the continuous distribution of flakes throughout the substrate and the average area of flakes ≈ 0.2 μm^2 as confirmed by scanning electron microscopy (SEM) and transmission electron microscopy (TEM) analysis. Swift heavy-ion (SHI) irradiation at 60, 100, and 150 MeV ion energies of 1×10^{12} ions/cm² ion fluence have been used to modify the band gap in few-layer MoS₂. The ions with two different energies are chosen at two sides of the Bragg peak of energy loss curve in such a way as to have the same value of electronic energy loss (S_e) but different ion energies to examine the velocity effect for the ion-induced modification. The absorbance peaks for 60 and 150 MeV irradiated samples show the same effect in the band gap modification.

1. INTRODUCTION

The creation of a MoS₂-based rapid light sensor and photo-detector was driven by the material's promising electrical and optical capabilities.^{1,2} A single layer of MoS₂ possesses a high band gap of 1.8 eV,³ whereas bulk MoS₂ has a band gap of 1.2 eV, showing layer-dependent band structural properties.⁴ In addition, it is worth noting that MoS₂ exhibits a structural phase dependence. For instance, the 2H (hexagonal) phase has a semiconducting behavior, whereas the 1T (trigonal) phase exhibits a metallic nature.⁵ The synthesis of monolayer and few-layer MoS₂, as well as the modification of electronic and optical band properties, are critical for high-potential applications for electronics and optoelectronics.⁶ According to some theoretical studies, devices built on thin-layer MoS₂ might have better transfer properties than silicon-based devices.^{7–10} Mechanical exfoliation,¹¹ solution casting,^{12,13} physical vapor deposition (PVD),^{14,15} and chemical vapor deposition (CVD)^{16,17} methods have been used for synthesizing mono and few layers of MoS₂. Among these, the CVD is the most effective method for growing uniform and high-crystalline MoS₂ films and 2D-MoS_{2(1-x)}Se_{2x} semiconductor alloy.¹⁸ It requires high temper-

ature and long preparation time.^{16,17} However the CVD preparation of MoS₂ has not been optimized for large-scale synthesis and it is not commonly used. Recently, researchers have been investigating the use of alkali halides to reduce the evaporation temperature of transition metal trioxide precursors, thereby reducing the high-temperature requirement in the CVD method. Various methods such as plasma immersion,¹⁹ laser irradiation,²⁰ and ion beam irradiation^{21,22} can be used to modify the electronic and optical band gap properties of few-layer MoS₂ for potential applications.^{11,23,24} Our group has investigated the effects of ion beam irradiation-induced modification of nanostructures, nanocomposites thin films, and 2D materials.^{25–37}

Received: July 20, 2023

Revised: November 5, 2023

Accepted: November 10, 2023

Published: November 27, 2023



In this report, we used a NaCl alkali halide-aided CVD technique to produce a few layers of MoS₂ on a quartz substrate. A high crystalline, homogeneous, and defect-free NaCl-assisted few-layer MoS₂ film was observed by using Raman spectroscopy. The electrical and optical characteristics of few-layer MoS₂ were modified by irradiation with swift heavy ions (SHI). The influence of ion velocity on ion-induced modification during the passage of ions through few-layer MoS₂ is studied. The same electronic energy loss S_e (from the leading and trailing side of the Bragg peak) at two different energies, 60 and 150 MeV, results in different ion velocities (as shown in Table 1) and has been chosen for study at the fluence of 1×10^{12} ions/cm².

Table 1. Ion Energy, Electronic Energy Loss (S_e), Nuclear Energy Loss (S_n), and Ion Velocity at Different Energies

ion energy (MeV)	electronic energy loss S_e (keV/nm)	nuclear energy loss S_n (keV/nm)	ion velocity (normalized to c , where $c = 3 \times 10^8$ m/s)
60	~11.0	~0.03	4.7×10^{-2}
100	~11.3	~0.02	6.0×10^{-2}
150	~11.0	~0.02	7.4×10^{-2}

2. EXPERIMENTAL SECTION

2.1. Synthesis. MoS₂ film was synthesized on a cleaned quartz substrate. The MoO₃ (Alfa Aesar 99.9%) and S (Alfa Aesar 99.9%) powders were used as the precursors in a self-assembled alumina-tube-assisted CVD system. At lowered temperature and atmospheric pressure (Figure S1a), a few-layer MoS₂ film was grown by combining NaCl powder with molybdenum trioxide (MoO₃) powder with 1:2 ratio (10 mg NaCl and 20 mg MoO₃) in one crucible positioned in the middle (650 °C) of a CVD furnace (see Figure S1a,b), whereas, the 100 mg sulfur (S) powder was placed in another crucible away from the middle by 16 cm at 120 °C temperature. The temperature profile and Ar gas flow throughout the growth process are described in Figure S1b. The evaporation temperature, relative location, gas flow, and growth duration for attaining the few-layer MoS₂ on quartz were optimized for good quality of the film.

2.2. Ion Beam Irradiation. The ion irradiation studies were carried out on CVD-grown few-layer MoS₂ using a 15-UD Pelletron Accelerator. The Ni ions of 60, 100, and 150 MeV were employed for irradiation studies under ambient temperature and a 10^{-6} mbar chamber pressure, with an ion fluence of 1×10^{12} ions/cm² at material science beamline (Beam Hall-I) IUAC, New Delhi. To minimize charging and overheating of targets, 0.5 particle nanoampere (pnA) beam current is used for irradiation. The Stopping and Range of Ions in Matter (SRIM) code has been used to determine electronic energy loss (S_e) and nuclear energy loss (S_n).³⁸ The experiments were conducted to observe the effect of ion velocity on band gap properties of few-layer MoS₂ having similar energy loss per unit length in a whole 1×1 cm² sample. The energy of Ni ions was chosen in such a way that energy loss per nm in the MoS₂ lies in the symmetry of the Bragg's curve (top of the peak at ~11.3 keV/nm, leading and trailing edges of the peak at ~11.0 keV/nm). The ratio of S_n and S_e values for a given energy from Table 1 shows that the effect of S_n in the MoS₂ samples is almost negligible as compared to S_e . However, the estimated defect densities of 60, 100, and 150 MeV Ni-ion-irradiated samples due to S_n using Transport of Ions in Matter (TRIM) software at a 1×10^{12} ions/cm² fluence are 1.97×10^{14} /cm², 0.92×10^{14} /cm², and 0.77×10^{14} /cm²,

respectively, which have been simulated for a 4 nm MoS₂ film on a quartz substrate. However, the defect density by S_e is not possible to estimate at the current state of our knowledge.

2.3. Characterization Techniques. An InVia Renishaw micro-Raman system with a confocal microscope objective of 50× and 514 nm excitation wavelength (Ar-ion laser) has been used to perform Raman scattering measurements, a back-scattering geometry at ambient temperature associated with a charge-coupled device detector. The optical absorbance of synthesized MoS₂ films was measured using a Hitachi U-3300 UV–visible spectrometer. The UV–vis data have been recorded with 1 nm interval with 1 nm resolution; however, the UV–vis measurements were also performed in the circular region of 3 mm diameter and recorded the average spectra. The XRD patterns were recorded using a standard X-ray source-based Bruker D8-Advance X-ray diffractometer with Cu K α ($\lambda = 1.54$ Å). The employed X-ray source was operated with 40 keV and 40 mA, and XRD patterns were recorded from 10 to 50° using a scintillator detector having a scan rate of 1°/min. Optical microscopes have the potential to serve as a rapid characterization facility for the identification of TMD films from the substrates. A Zeiss Light optical microscope has been used to characterise the film in this instance. The surface pictures of the few-layer MoS₂ film were captured using a Tescan MIRA II field emission scanning electron microscope at 15 keV electron energy. The topography of the surface and the number of layers of MoS₂ grown on the substrate were measured using the tapping mode of a Digital Instruments Nanoscope-III atomic force microscope (AFM) with an inflexible cantilever. Transmission electron microscopy (TEM) and high-resolution TEM (HRTEM) were used to explore the nanostructural characteristics of a deposited few-layer MoS₂ sample using a JEM F200 (JEOL) TEM with a 200 kV field emission gun. The thickness of the film and elemental concentration were estimated by Rutherford backscattering spectroscopy (RBS) using a 2 MeV He⁺ ion beam.

3. RESULTS AND DISCUSSION

3.1. Growth Mechanism. Few-layer MoS₂ were synthesized at 650 °C with the help of NaCl according to the protocol of a recent report by Zhang et al.³⁹ The growth process of few-layer MoS₂ by utilizing NaCl still needs to be understood, which is important for reducing the high-temperature requirement challenge in CVD. The synthesized samples, both unwashed (pristine) and treated with DI water (washed), were thoroughly examined by characterization techniques. The alkali halide NaCl causes the creation of intermediate product MoO₂Cl₂,⁴⁰ which can quicken the growth of MoS₂ and open the door to interactions between MoO₂Cl₂ and sulfur in the gas phase. MoO₂Cl₂ has a lower evaporation temperature than MoO₃, which lowers the growth temperature of the CVD process (see the chemical reactions as shown in eqs 1 and 2 in the Supporting Information). It can increase the nucleation density and therefore the mass flow of the metal precursors. The use of a modest amount of MoO₃ powder prevents overnucleation. Finally, we get water-soluble Na₂SO₄ and Na₂S supplementary products with a few layers of MoS₂ by the NaCl-aided growth procedure.⁴¹ Consequently, the analysis of the few-layer MoS₂ film has been performed utilizing the above-mentioned characterization techniques.

3.2. Raman Spectroscopy. Raman peaks at 147, 229.5, and 288.1 cm⁻¹ corresponding to Na₂S, and peaks at 601.8, 753.4, and 901 cm⁻¹ corresponding to Na₂SO₄ were observed [Figure

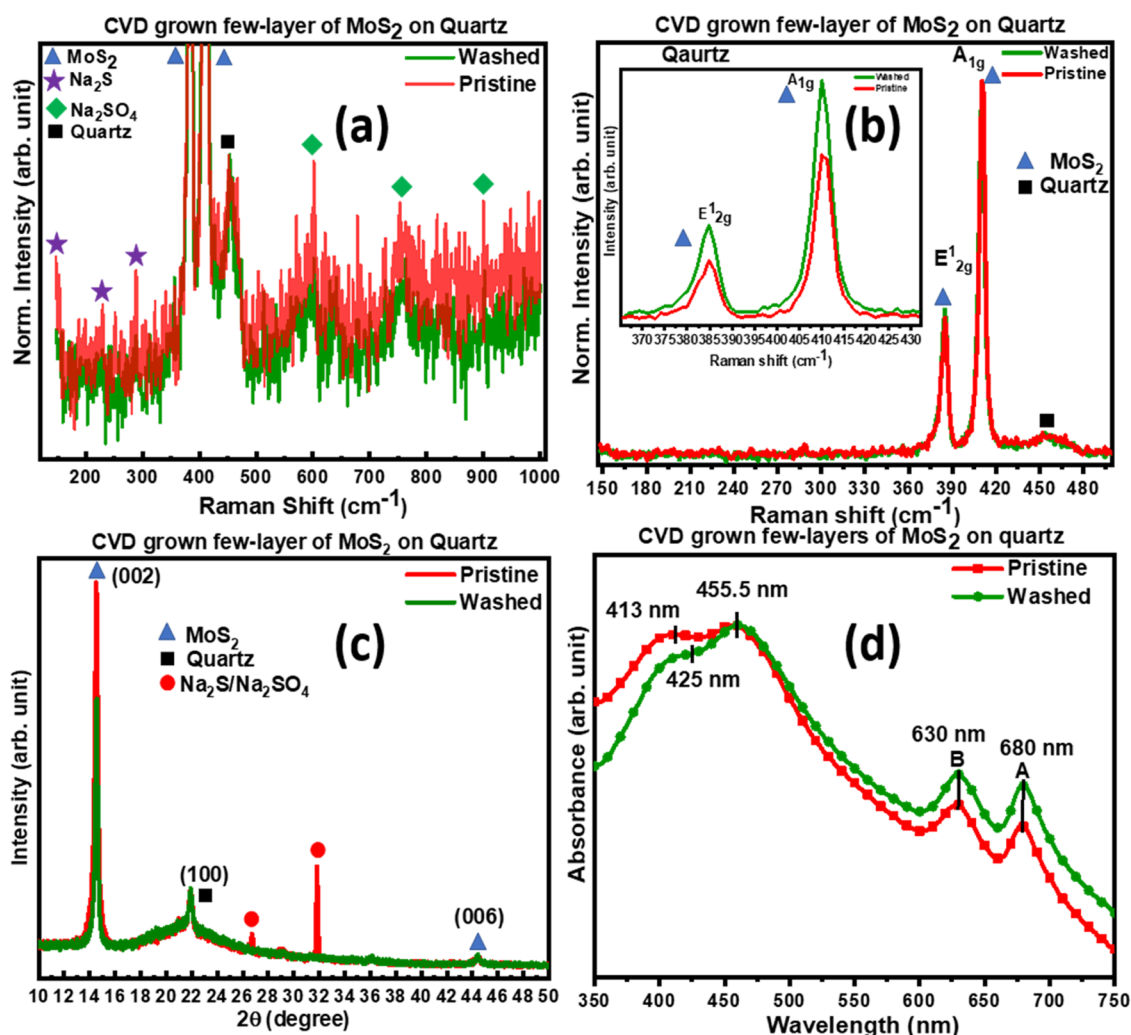


Figure 1. (a) Full-range Raman spectra of few-layer MoS₂, (b) selected-range Raman spectra of few-layer MoS₂, (c) XRD plot, and (d) UV–vis spectra of pristine and washed few-layer MoS₂.

1a,b], while the high-intensity peaks close to 400 cm⁻¹ are E¹_{2g} (385 cm⁻¹) and A_{1g} (409.5 cm⁻¹) represent MoS₂. The systematic study of pristine and washed few-layer MoS₂ shows a significant change in the results. Especially in the observed characteristic signal of Raman spectroscopy and XRD (peak at 2θ ≈ 27 and 32°), the washed few-layer MoS₂ sample is free from the associated compounds such as Na₂S and Na₂SO₄ because the peaks observed related to the Na₂S and Na₂SO₄ are wiped out [see Figure 1a,c]. In UV–vis spectroscopy (Figure 1d), unlike Raman and XRD, no specific peak appears corresponding to the Na₂S and Na₂SO₄ compounds. However, a significant absorbance enhancement was observed for washed sample.

The difference in peak positions between A_{1g} and E¹_{2g} is 24.5 cm⁻¹, agreed to the few-layer (2L–5L monolayers) MoS₂,⁴² which is also shown by AFM sectional analysis in a section below. However, the area of the Raman peaks and positions are the same for both washed and pristine few-layer MoS₂, which signifies that the original quality of the sample was unchanged, which is highly desirable for application studies.

3.3. XRD and UV–Vis Spectroscopy. Figure 1c shows the identical XRD patterns of the pristine and washed few-layer MoS₂ film on the quartz substrate. The diffraction peaks were observed at 2θ ≈ 14.52 and 44.44°, which corresponded to the

(002) and (006) planes of MoS₂ (JCPDS 37-1492), respectively. UV–vis absorbance measurements of pristine and washed few-layer MoS₂ are shown in Figure 1d. The obtained spectra display two eminent absorbance peaks A at 680 nm (1.82 eV) and B at 630 nm (1.96 eV) corresponding to the excitonic absorbance bands.^{3,12} These bands are the result of spin–orbit interaction at the K-symmetry point, which caused valence band splitting and energy difference of A and B excitonic peaks matches with respective valence band splitting values.¹² This observation provides evidence of the characteristic optical, electrical, and homogeneous layered properties of few-layer MoS₂. Besides, consistency with the MoS₂ theoretical band structure provides strong support for claiming good crystal quality MoS₂ films. The optical image of the few-layer MoS₂ film shown in Figure S2a exhibits a consistent contrast in color on the substrate that signifies the uniform thickness, which has almost full coverage of MoS₂ film on the substrate.

3.4. RBS Spectrometry. The film thickness of the sample was determined by using Rutherford backscattering spectrometry (RBS), as seen in Figure 2. The obtained results indicate that the film thickness measures 4 nm. It is also agreed with Raman spectroscopy results that the grown films lie between 2L and 5L. Furthermore, it is worth noting that the measured stoichiometry of the Mo/S atoms in the sample is in a 1:2 ratio,

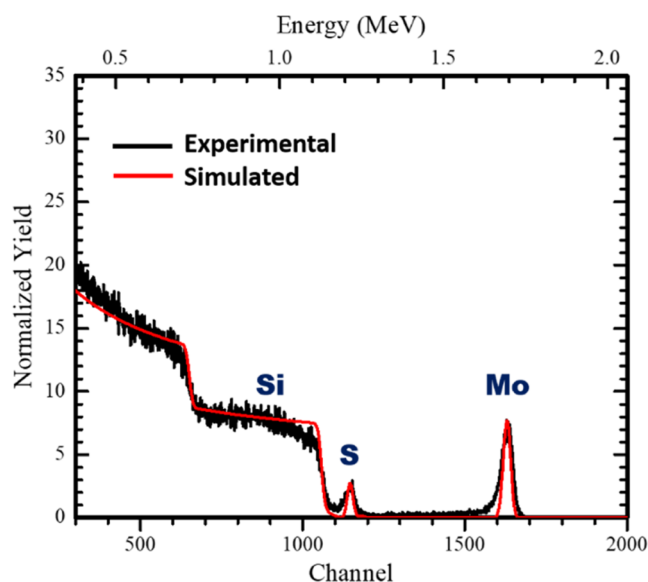


Figure 2. RBS spectra of CVD-grown few-layer MoS₂.

indicating a high level of sample quality in terms of stoichiometry.

3.5. SEM, AFM, and TEM Microscopy. The SEM image of the few-layer MoS₂ film is shown in Figure S2b. The distribution of the triangular-shaped MoS₂ flakes and their stacking on the substrate were also apparently visible, which again confirms the large-area growth of the few-layer MoS₂.

The edges of the layers are measured using AFM to determine the number of layers in few-layer MoS₂. The provided picture, Figure S2c, depicts an AFM image of MoS₂ flakes that were captured in tapping mode. The color representation in the image serves to indicate the level of homogeneity in the film thickness. Height profiles across the MoS₂ edge sample (Figure S2c) show that the thickness of our sample is about ≈ 1.7 to 4 nm (as seen in the height profiles at a different area of the samples in Figure S2c) corresponding to few-layer (2L–5L monolayer) MoS₂. The results of the AFM for the sample thickness measurement are in good agreement with the results of the other two different techniques, which are Raman spectroscopy and RBS spectrometry. TEM and HRTEM have been used to confirm the crystal structure of the 2D-MoS₂. The TEM sample was prepared by dripping a drop of water on the quartz substrate with a formed few layers of MoS₂. The flakes were then separated from the substrate and floated on top of a water droplet. To scoop the flakes, copper grids with porous carbon sheets were utilized.³⁹

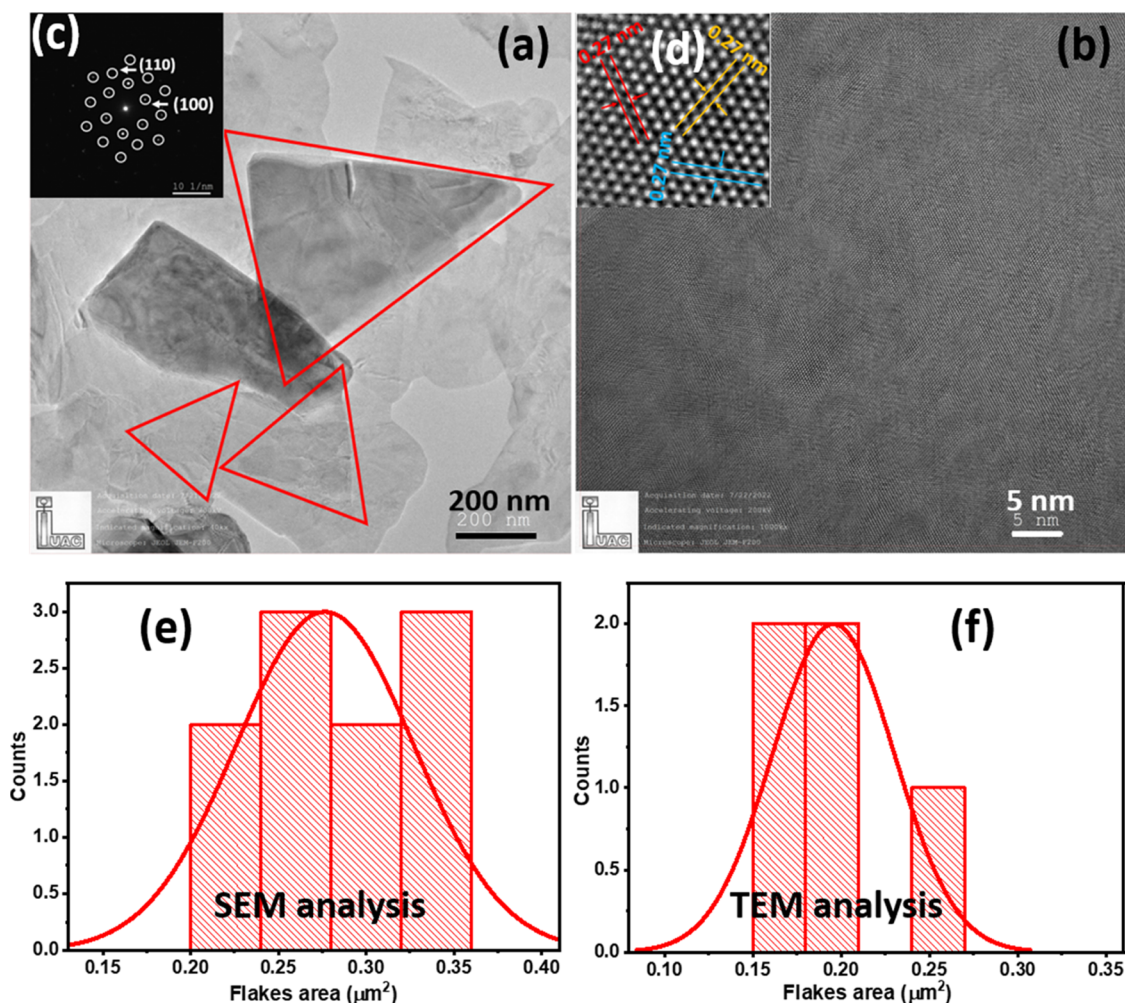


Figure 3. (a) TEM, (b) HRTEM, (c) SAED pattern, and (d) magnified HRTEM image of few-layer MoS₂. (e, f) Analysis of average flakes area using SEM image and TEM image of few-layer MoS₂.

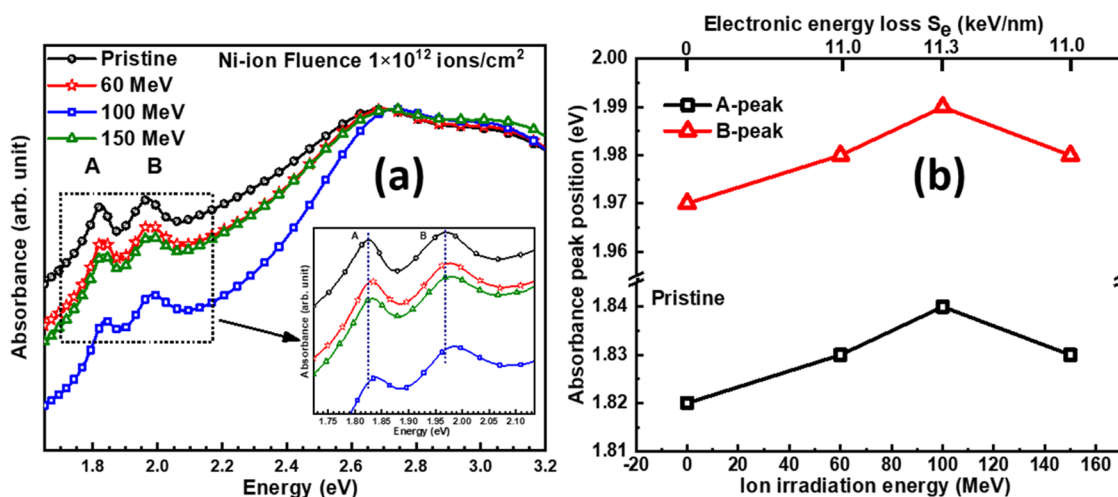


Figure 4. (a) UV–vis absorbance spectra of few-layer MoS₂ under Ni-ion irradiation at different energies with 1×10^{12} ions/cm² ion fluence and (b) absorbance peak shifting with irradiated ion energy and electronic energy loss of irradiated ions at 1×10^{12} ions/cm² ion fluence.

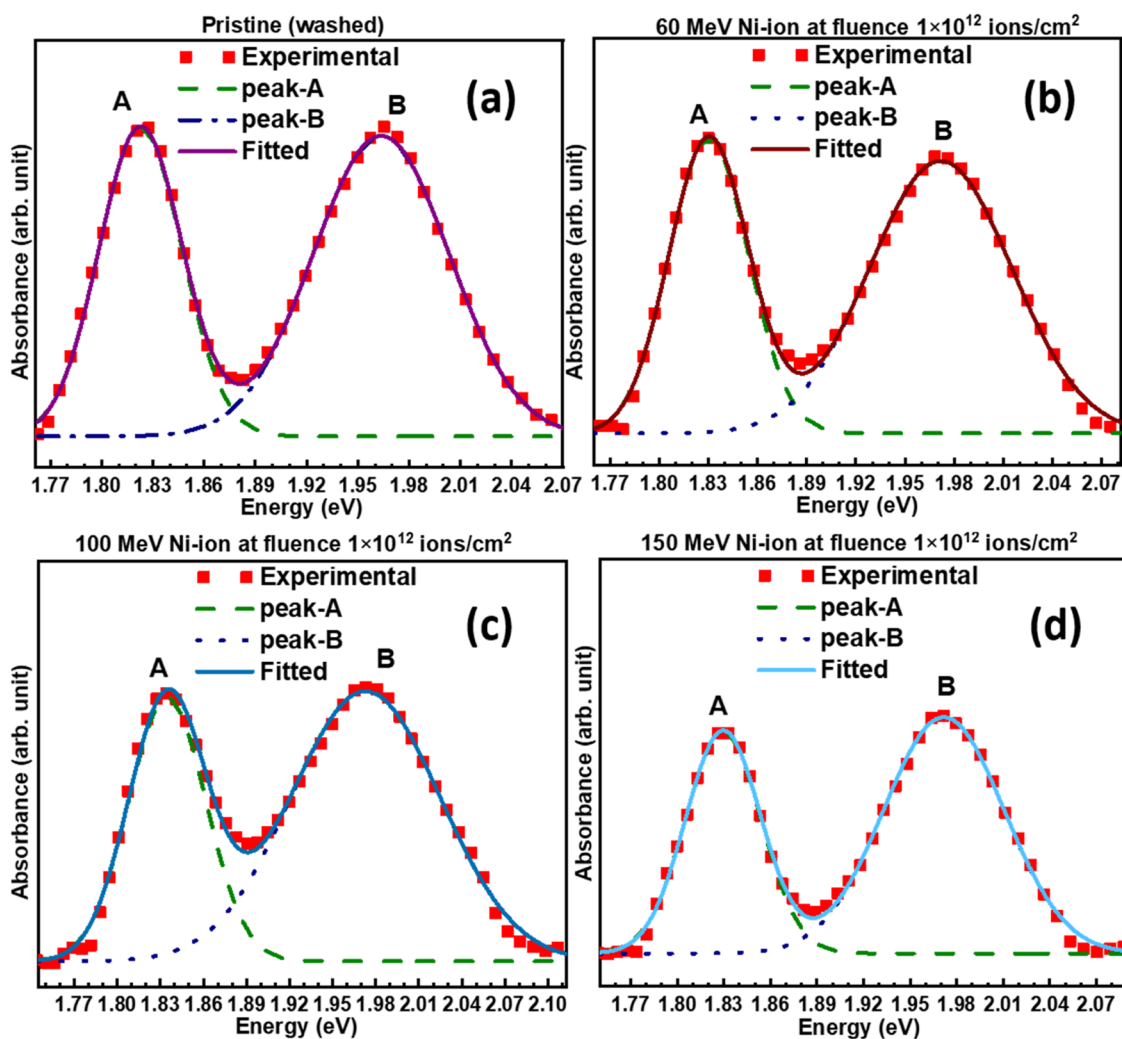


Figure 5. Deconvolution and peak fitting of A-peak and B-peak of UV–vis absorbance spectra for (a) pristine, (b) 60 MeV, (c) 100 MeV, and (d) 150 MeV Ni-ion-irradiated samples at fluence 1×10^{12} ions/cm².

TEM and HRTEM pictures in Figure 3a,b were taken from arbitrary regions of MoS₂ samples that had been exfoliated onto the TEM grid. The SAED pattern shown in Figure 3c and the HRTEM image shown in Figure 3d disclose the hexagonal

lattice structure of few-layer MoS₂. In addition, Figure 3d shows honeycomb arrangements of the Mo and S atoms. The SAED pattern was recorded at the marked area; the observed planes are (100) and (110) as shown in Figure 3c. The SAED pattern

Table 2. Band Gap Shifts due to the Compressive Strain Caused by Different Inducing Conditions, Including Irradiation

strain induced by	energy	type of strain	band gap shifts	reference
Au-ion irradiation	500 keV	compressive	~38 meV	47
He-ion irradiation	1.66 MeV	compressive	blue-shifting	48
γ -irradiation (Co-60)	~1.25 MeV	compressive	blue-shifting	50
γ -irradiation (Co-60)	~1.25 MeV	compressive	~44 meV	51
e-beam irradiation	15 keV	compressive	40–50 meV	52
electromechanical devices		compressive	~60 meV	45

illustrates the single-crystalline nature of the grown MoS₂ film whose interplanar spacing d is 0.27 nm, which matches with HRTEM, and is consistent with the previous reports.¹⁶ The average area of the flakes determined from SEM image analysis is $\approx 0.275 \mu\text{m}^2$, as shown in Figure 3e, which is close to the TEM analysis result (Figure 3f) $\approx 0.200 \mu\text{m}^2$. However, the difference in the average area of the MoS₂ flakes may be caused by the exfoliation of the CVD-grown sample from the substrate to the TEM grid. Though handling in the transfer process was very careful, there are still chances that unwanted force or strain may be responsible for the discrepancy.

3.6. Ion Beam Modification and Ion Velocity Effect on the Band Gap. In the ion beam-assisted modification process, one can tune the photoabsorbance properties in a controlled manner by controlling the density of the defects with ion fluence.^{11,21,43} Additionally, the utilization of ion beam-assisted modification techniques becomes advantageous in terms of altering the properties of a specific location within the sample. Figure 4a,b displays the UV–vis spectra of the few-layer MoS₂ with different ion beam energies (60, 100, and 150 MeV) with a fluence of 1×10^{12} ions/cm². However, the observed spectra of each sample have been deconvoluted and Gaussian fitted for a better understanding of the UV–vis spectra modification under ion beam irradiation, which are shown in Figure 5a–d. The first peak of the absorbance vs energy plot represents the band gap in 2D materials, as described by Sahoo et al.⁴⁴ The plots of absorbance vs energy for pristine and irradiated samples at different energies are shown in Figure 4a. This Ni ion with 60 and 150 MeV has approximately the same electronic energy loss (11.0 keV/nm) in the few-layer MoS₂ and shows an almost similar optical absorbance peak position at 1×10^{12} ions/cm², as shown in Figure 4a,b. This shows the optical band gap is not dependent on ion velocity (see A-peak from Figure 4b). It is expected from the velocity effect that if the two ions have the same S_e value but different ion velocities by choosing the ions at the two sides of the Bragg's peak, the slower ion produces more damage or modification in the sample. In the present experiment, the ions with the same S_e with different velocities have almost the same effect on the band gap, and therefore, it contradicts the velocity effect for the band gap. The intensity of the absorbance spectra is modified, as shown in Figure 4a for peaks A and B at different ion energies. The electronic energy loss of 100 MeV Ni ions is 11.3 keV/nm, which is the maximum energy loss value among all energies. As a result, the absorbance spectra of the 100 MeV Ni ion irradiated sample show maximum intensity modification (see Figure 4a), as well as maximum A-peak and B-peak shifting (see Figure 4b). Among these three Ni ion energies, 100 MeV Ni ion irradiation is significant for the optical property modification in few-layer MoS₂. The RBS measurements of the pristine and irradiated samples have been performed for the estimation of the sulfur vacancies. The atomic concentration of S and Mo atoms in the sample is proportional to the area under their respective peak in the RBS spectra, where

the atomic concentration for each element is calculated by dividing the integrated counts below the Mo and S peaks by their respective Rutherford cross sections. Here, the atomic concentrations of S and Mo elements were denoted by Y_S and Y_{Mo} , respectively. The stoichiometry can be obtained by the ratio Y_S/Y_{Mo} . The plot between the Y_S/Y_{Mo} vs ion energy, which is shown in Figure S3, reveals a significant change in stoichiometry under ion irradiation. This shows the decrease in the Y_S/Y_{Mo} ratio of irradiated samples compared to pristine samples, implying sulfur deficiency resulting from preferential sputtering of the S atoms.

The observed blue-shifting in the A and B peaks of the optical spectra is caused by the compressive strain produced by ion irradiation. It has been shown by theoretical studies by Hui et al.⁴⁵ and Burns et al.⁴⁶ that compressive strain causes blue shift. The earlier experiments also suggested that ion irradiation,^{47–49} γ irradiation,^{50,51} and electron irradiation⁵² produce sulfur vacancies. The sulfur vacancies produced by various methods cause compressive strain on the lattice structure.^{47–52} The band gap shifts due to the compressive strain caused by different inducing conditions, including irradiation, are given in Table 2. In this study, sulfur deficiency due to preferential sputtering of sulfur under ion irradiation has been observed from the RBS as shown in Figure S3. This is responsible for inducing the compressive strain in the lattice structure of MoS₂ under ion irradiation, which causes the blue shifts in the irradiated sample spectra as compared to pristine. This is well consistent with our earlier theoretical study that showed a blue shift of the MoS₂ band gap under applied compressive biaxial strain.³ In addition, this is in agreement with other reports.^{45,46}

4. CONCLUSIONS

In summary, a simple CVD method is explored to produce high-quality few-layer MoS₂ at a relatively lower temperature with less than 5 layers of MoS₂, as confirmed by AFM, RBS, and Raman measurements. In addition, the synthesis mechanism has been investigated by Raman, UV–vis, and XRD measurements. The optical image shows the continuous distribution of flakes throughout the substrate, and the average area of flakes $\approx 0.2 \mu\text{m}^2$ was confirmed by SEM and TEM analysis. The SAED pattern illustrates the single-crystalline nature of the grown MoS₂ film, whose interplanar spacing d is 0.27 nm. Additionally, the band gap of a few-layer MoS₂ has been marginally modified (20 meV) by 100 MeV Ni ions having an S_e of 11.3 keV/nm, which has been observed due to strain induced by ion irradiation. The band gaps for the MoS₂ samples irradiated by 60 and 150 MeV have the same S_e , indicating that the velocity effect is not playing any role in band gap modification.

■ ASSOCIATED CONTENT

Data Availability Statement

The data that support the findings of this study are available from the corresponding authors upon reasonable request.

Supporting Information

The Supporting Information is available free of charge at <https://pubs.acs.org/doi/10.1021/acsomega.3c05240>.

Synthesis technique as well as microscopic properties, including optical microscopy, scanning electron microscopy (SEM), and atomic force microscopy (AFM); examination and analysis of the phenomenon of defect creation by sulfur sputtering under ion irradiation utilizing Rutherford backscattering spectrometry (RBS) observations (PDF)

AUTHOR INFORMATION

Corresponding Author

Mayur Khan – Materials Science Group, Inter-University Accelerator Centre, New Delhi 110067, India; orcid.org/0000-0002-9313-0482; Email: khanmayur253@gmail.com

Authors

Ramcharan Meena – Materials Science Group, Inter-University Accelerator Centre, New Delhi 110067, India

Devesh Kumar Avasthi – Centre for Interdisciplinary Research, University of Petroleum and Energy Studies, Dehradun 248007 Uttarakhand, India

Ambuj Tripathi – Materials Science Group, Inter-University Accelerator Centre, New Delhi 110067, India; orcid.org/0000-0002-1240-5836

Complete contact information is available at <https://pubs.acs.org/10.1021/acsomega.3c05240>

Author Contributions

M.K.: Data curation, conceptualization, formal analysis, methodology, writing—original draft (equal) and editing. R.M.: Data curation, resources. D.K.A.: Conceptualization, writing—review and editing. A.T.: Resources, conceptualization, writing—review and editing, supervision.

Notes

The authors declare no competing financial interest.

ACKNOWLEDGMENTS

The Council of Scientific and Industrial Research (CSIR), New Delhi, India, is acknowledged for providing a fellowship to M.K., with the EMR file number 09/760(0039)/2019-EMR-I. The authors also acknowledge Sanjay Kedia for the XRD measurements, Prof. Shyama Rath for the Raman measurement, and Sunil Ojha and G.R. Umopathy for RBS measurement. Additionally, Dr. S. A. Khan, Dr. Indra Sulania, and Ambuj Mishra provided SEM, AFM, and TEM measurements, respectively. The authors thank the Pelletron team for supplying the beam. They also acknowledge Department of Science and Technology for providing SEM under Nano Mission program. They are grateful to the Pelletron group for providing the stable beam current during the irradiation experiment.

REFERENCES

- (1) Li, T.; Galli, G. Electronic properties of mos2 nanoparticles. *J. Phys. Chem. C* **2007**, *111*, 16192–16196.
- (2) Mak, K. F.; Shan, J. Photonics and optoelectronics of 2d semiconductor transition metal dichalcogenides. *Nat. Photonics* **2016**, *10*, 216–226.
- (3) Khan, M.; Tripathi, M. N.; Tripathi, A. Strain-induced structural, elastic, and electronic properties of 1l-mos2. *J. Mater. Res.* **2022**, *37*, 3340–335.
- (4) Kuc, A.; Zibouche, N.; Heine, T. Influence of quantum confinement on the electronic structure of the transition metal sulfide TS₂. *Phys. Rev. B* **2011**, *83*, No. 245213.
- (5) Wang, Y.-Y.; Deng, J.-J.; Wang, X.; Che, J.-T.; Ding, X.-L. Small stoichiometric (MoS₂)_n clusters with the 1T-phase. *Phys. Chem. Chem. Phys.* **2018**, *20*, 6365–6373.
- (6) Kumbhakar, P.; Chowde Gowda, C.; Tiwary, C. S. Advance optical properties and emerging applications of 2d materials. *Front. Mater.* **2021**, *8*, No. 721514.
- (7) Rahmati, B.; Ghayeb-Zamharir, S.; Karimzadeh, R.; Mohseni, S. M. Nonlinear optical properties of vertically-aligned mos2 nanosheets. *J. Electron. Mater.* **2021**, *50*, 3645–3651.
- (8) Lin, Y.-C.; Dumcenco, D. O.; Huang, Y.-S.; Suenaga, K. Atomic mechanism of the semiconducting-to-metallic phase transition in single-layered mos2. *Nat. Nanotechnol.* **2014**, *9*, 391–396.
- (9) Klein, J.; Sigl, L.; Gyger, S.; Barthelmi, K.; Florian, M.; Rey, S.; Taniguchi, T.; Watanabe, K.; Jahnke, F.; Kastl, C.; et al. Engineering the luminescence and generation of individual defect emitters in atomically thin mos2. *ACS Photonics* **2021**, *8*, 669–677.
- (10) Zhang, E.; Wang, W.; Zhang, C.; Jin, Y.; Zhu, G.; Sun, Q.; Zhang, D. W.; Zhou, P.; Xiu, F. Tunable charge-trap memory based on few-layer MoS₂. *ACS Nano* **2015**, *9*, 612–619.
- (11) Jeffery, A. A.; Nethravathi, C.; Rajamathi, M. Two-dimensional nanosheets and layered hybrids of MoS₂ and WS₂ through exfoliation of ammoniated MS₂ (M= Mo, W). *J. Phys. Chem. C* **2014**, *118* (2), 1386–96.
- (12) Khan, M.; Kumar, S.; Mishra, A.; Sulania, I.; Tripathi, M. N.; Tripathi, A. Study of structural and electronic properties of few-layer MoS₂ film. *Mater. Today: Proc.* **2022**, *57*, 100–105.
- (13) Khan, M.; Kedia, S. K.; Mishra, A.; Avasthi, D. K.; Tripathi, A. Investigation of the annealing temperature for few-layer MoS₂ and ion beam-induced athermal annealing/purification behaviour by in-situ XRD. *Appl. Surf. Sci.* **2023**, *639*, No. 158106.
- (14) Choudhary, N.; Park, J.; Hwang, J. Y.; Choi, W. Growth of large-scale and thickness-modulated MoS₂ nanosheets. *ACS Appl. Mater. Interfaces* **2014**, *6*, 21215–21222.
- (15) Gupta, N. K.; Barwal, V.; Pandey, L.; Hait, S.; Mishra, V.; Kumar, A.; Chaudhary, S. Growth of MoS₂ by controlled sulfurization of pulsed dc sputtered Mo-thin films. *AIP Conf. Proc.* **2020**, *2220*, No. 090023.
- (16) Singh, A.; Sharma, M.; Singh, R. NaCl-assisted CVD growth of large-area high-quality trilayer MoS₂ and the role of the concentration boundary layer. *Cryst. Growth Des.* **2021**, *21*, 4940–4946.
- (17) Chen, J.; Tang, W.; Tian, B.; Liu, B.; Zhao, X.; Liu, Y.; Ren, T.; Liu, W.; Geng, D.; Jeong, H. Y.; et al. Chemical vapor deposition of high-quality large-sized MoS₂ crystals on silicon dioxide substrates. *Adv. Sci.* **2016**, *3*, No. 1600033.
- (18) Yao, W.; Kang, Z.; Deng, J.; Chen, Y.; Song, Q.; Ding, X. L.; Lu, F.; Wang, W. Synthesis of 2D-MoS₂(1-x)Se_{2x} semiconductor alloy by chemical vapor deposition. *RSC Adv.* **2020**, *10*, 42172–42177.
- (19) Haynes, K.; Murray, R.; Weinrich, Z.; Zhao, X.; Chiappe, D.; Sutar, S.; Radu, I.; Hatem, C.; Perry, S.; Jones, K. Modulating the resistivity of MoS₂ through low energy phosphorus plasma implantation. *Appl. Phys. Lett.* **2017**, *110*, No. 262102.
- (20) Rani, R.; Dimple, Jena, N.; Kundu, A.; Sarkar, A. D.; Hazra, K. S. Controlled formation of nanostructures on MoS₂ layers by focused laser irradiation. *Appl. Phys. Lett.* **2017**, *110*, No. 083101.
- (21) Yudin, V. I.; Lozhkin, M. S.; Shurukhina, A. V.; Emeline, A. V.; Kapitonov, Y. V. Photoluminescence manipulation by ion beam irradiation in CsPbBr₃ halide perovskite single crystals. *J. Phys. Chem. C* **2019**, *123* (34), 21130–4.
- (22) Yamada, Y.; Takahashi, K.; Ikuta, T.; Nishiyama, T.; Takata, Y.; Ma, W.; Takahara, A. Tuning surface wettability at the submicron-scale: effect of focused ion beam irradiation on a self-assembled monolayer. *J. Phys. Chem. C* **2016**, *120* (1), 274–80.
- (23) Ghorbani-Asl, M.; Kretschmer, S.; Spearot, D. E.; Krashenninnikov, A. V. Two-dimensional MoS₂ under ion irradiation: from controlled defect production to electronic structure engineering. *2D Mater.* **2017**, *4*, No. 025078.

- (24) Singh, A.; Sharma, G.; Singh, B. P.; Vasa, P. Charge-induced lattice compression in monolayer MoS₂. *J. Phys. Chem. C* **2019**, *123* (29), 17943–50.
- (25) Kumar, S.; Tripathi, A.; Khan, S. A.; Pannu, C.; Avasthi, D. K. Radiation stability of graphene under extreme conditions. *Appl. Phys. Lett.* **2014**, *105*, No. 133107.
- (26) Tyagi, C.; Tripathi, A.; Dey, A. B.; Avasthi, D. K. Structural changes induced in graphene oxide film by low energy ion beam irradiation. *Radiat. Phys. Chem.* **2022**, *192*, No. 109923.
- (27) Ratan, A.; Kunchakara, S.; Dutt, M.; Tripathi, A.; Singh, V. Enhanced electrical properties of few layers MoS₂-PVA nanocomposite film via homogeneous dispersion and annealing effect induced by 80 MeV carbon 6⁺ swift heavy ion irradiation. *Mater. Sci. Semicond. Process.* **2020**, *108*, No. 104877.
- (28) Bajwa, N.; Ingale, A.; Avasthi, D. K.; Kumar, R.; Tripathi, A.; Dharamvir, K.; Jindal, V. Role of electron energy loss in modification of C₆₀ thin films by swift heavy ions. *J. Appl. Phys.* **2008**, *104*, No. 054306.
- (29) Bajwa, N.; Dharamvir, K.; Jindal, V.; Ingale, A.; Avasthi, D. K.; Kumar, R.; Tripathi, A. Swift heavy ion induced modification of C₆₀ thin films. *J. Appl. Phys.* **2003**, *94*, 326–333.
- (30) Kumar, A.; Avasthi, D. K.; Tripathi, A.; Kabiraj, D.; Singh, F.; Pivin, J. Synthesis of confined electrically conducting carbon nanowires by heavy ion irradiation of fullerene thin film. *J. Appl. Phys.* **2007**, *101*, No. 014308.
- (31) Kumar, A.; Avasthi, D. K.; Pivin, J.; Tripathi, A.; Singh, F. Ferromagnetism induced by heavy-ion irradiation in fullerene films. *Phys. Rev. B* **2006**, *74*, No. 153409.
- (32) Kumar, A.; Avasthi, D. K.; Pivin, J.; Koinkar, P. Ordering of fullerene and carbon nanotube thin films under energetic ion impact. *Appl. Phys. Lett.* **2008**, *92*, No. 221904.
- (33) Mishra, Y. K.; Singh, F.; Avasthi, D. K.; Pivin, J.; Malinowska, D.; Pippel, E. Synthesis of elongated Au nanoparticles in silica matrix by ion irradiation. *Appl. Phys. Lett.* **2007**, *91*, No. 063103.
- (34) Mishra, Y. K.; Avasthi, D. K.; Kuliya, P.; Singh, F.; Kabiraj, D.; Tripathi, A.; Pivin, J.; Bayer, I.; Biswas, A. Controlled growth of gold nanoparticles induced by ion irradiation: An in-situ X-ray diffraction study. *Appl. Phys. Lett.* **2007**, *90*, No. 073110.
- (35) Avasthi, D. K.; Mishra, Y.; Singh, F.; Stoquert, J. Ion tracks in silica for engineering the embedded nanoparticles. *Nucl. Instrum. Methods Phys. Res., Sect. B* **2010**, *268*, 3027–3034.
- (36) Kumar, S.; Tripathi, A.; Singh, F.; Khan, S. A.; Baranwal, V.; Avasthi, D. K. Purification/annealing of graphene with 100-MeV Ag ion irradiation. *Nanoscale Res. Lett.* **2014**, *9*, 126.
- (37) Tyagi, C.; Khan, S.; Sulania, I.; Meena, R.; Avasthi, D. K.; Tripathi, A. Evidence of ion-beam-induced annealing in graphene oxide films using in situ X-ray diffraction and spectroscopy techniques. *J. Phys. Chem. C* **2018**, *122*, 9632–9640.
- (38) Ziegler, J. F.; Biersack, J. P. The Stopping and Range of Ions in Matter. In *Treatise on Heavy-Ion Science*; Springer, 1985; pp 93–129.
- (39) Zhang, L.; Wang, C.; Liu, X.-L.; Xu, T.; Long, M.; Liu, E.; Pan, C.; Su, G.; Zeng, J.; Fu, Y.; et al. Damage-free and rapid transfer of CVD-grown two-dimensional transition metal dichalcogenides by dissolving sacrificial water-soluble layers. *Nanoscale* **2017**, *9*, 19124–19130.
- (40) Li, J.; Yan, W.; Lv, Y.; Leng, J.; Zhang, D.; Coileáin, C. O.; Cullen, C. P.; Stimpel-Lindner, T.; Duesberg, G. S.; Cho, J.; et al. Sub-millimeter size high mobility single crystal MoSe₂ monolayers synthesized by NaCl-assisted chemical vapor deposition. *RSC Adv.* **2020**, *10*, 1580–1587.
- (41) Bharmoria, P.; Gehlot, P. S.; Gupta, H.; Kumar, A. Temperature-dependent solubility transition of Na₂SO₄ in water and the effect of NaCl therein: solution structures and salt water dynamics. *J. Phys. Chem. B* **2014**, *118*, 12734–12742.
- (42) Balendhran, S.; Ou, J. Z.; Bhaskaran, M.; Sriram, S.; Ippolito, S.; Vasic, Z.; Kats, E.; Bhargava, S.; Zhuiykov, S.; Kalantar-Zadeh, K. Atomically thin layers of MoS₂ via a two-step thermal evaporation-exfoliation method. *Nanoscale* **2012**, *4*, 461–466.
- (43) Kim, D.; Du, H.; Kim, T.; Shin, S.; Kim, S.; Song, M.; Lee, C.; Lee, J.; Cheong, H.; Seo, D. H.; Seo, S. The enhanced low resistance contacts and boosted mobility in two-dimensional p-type WSe₂ transistors through Ar⁺ ion-beam generated surface defects. *AIP Adv.* **2016**, *6*, No. 105307.
- (44) Sahoo, D.; Kumar, B.; Sinha, J.; Ghosh, S.; Roy, S. S.; Kaviraj, B. Cost-effective liquid phase exfoliation of mos2 nanosheets and photocatalytic activity for wastewater treatment enforced by visible light. *Sci. Rep.* **2020**, *10*, No. 10759.
- (45) Hui, Y. Y.; Liu, X.; Jie, W.; Chan, N. Y.; Hao, J.; Hsu, Y.-T.; Li, L.-J.; Guo, W.; Lau, S. P. Exceptional tunability of band energy in a compressively strained trilayer MoS₂ sheet. *ACS Nano* **2013**, *7*, 7126–7131.
- (46) Burns, K.; Tan, A. M. Z.; Gordon, V. H.; Wang, T.; Gabriel, A.; Shao, L.; Hennig, R. G.; Aitkaliyeva, A. Strain modulation using defects in two-dimensional MoS₂. *Phys. Rev. B* **2020**, *102*, No. 085421.
- (47) He, Z.; Zhao, R.; Chen, X.; Chen, H.; Zhu, Y.; Su, H.; Huang, S.; Xue, J.; Dai, J.; Cheng, S.; et al. Defect engineering in single-layer MoS₂ using heavy ion irradiation. *ACS Appl. Mater. Interfaces* **2018**, *10*, 42524–42533.
- (48) Isherwood, L. H.; Worsley, R. E.; Casiraghi, C.; Baidak, A. Alpha particle irradiation of bulk and exfoliated MoS₂ and WS₂ membranes. *Nucl. Instrum. Methods Phys. Res., Sect. B* **2018**, *435*, 180–189.
- (49) Mahanta, T.; Shakya, J.; Mohanty, T. Evolution of Raman spectra in ion irradiated MoS₂ atomic layers: Computational and experimental studies. *J. Nanosci. Nanotechnol.* **2020**, *20*, 7522–7529.
- (50) Singh, A.; Singh, R. γ -ray irradiation-induced chemical and structural changes in CVD monolayer MoS₂. *ECS J. Solid-State Sci. Technol.* **2020**, *9*, No. 093011.
- (51) Isherwood, L. H.; Athwal, G.; Spencer, B. F.; Casiraghi, C.; Baidak, A. Gamma radiation-induced oxidation, doping, and etching of two-dimensional MoS₂ crystals. *J. Phys. Chem. C* **2021**, *125* (7), 4211–22.
- (52) Matsunaga, M.; Higuchi, A.; He, G.; Yamada, T.; Kruger, P.; Ochiai, Y.; Gong, Y.; Vajtai, R.; Ajayan, P. M.; Bird, J. P.; Aoki, N. Nanoscale-barrier formation induced by low-dose electron-beam exposure in ultrathin MoS₂ transistors. *ACS Nano* **2016**, *10*, 9730–9737.